Bull. Mater. Sci., Vol. 40, No. 5, September 2017, pp. 933–938
DOI 10.1007/s12034-017-1455-4
© Indian Academy of Sciences

Role of MnO in manganese–borate binary glass systems: a study on structure and thermal properties

T LEWANDOWSKI*, M ŁAPIŃSKI, M WALAS, M PRZEŚNIAK-WELENC and L WICIKOWSKI
Department of Solid State Physics, Gdansk University of Technology, 80-233 Gdansk, Poland
*Author for correspondence (tlewandowski@mif.pg.gda.pl)

MS received 24 July 2016; accepted 23 November 2016; published online 30 August 2017

Abstract. Structural and thermal properties of $x\mathrm{MnO}-(100-x)\mathrm{B_2O_3}$ (where $x = 40$, 50 and 60 mol%) glass samples have been investigated with the employment of various techniques. Fourier transform infrared spectroscopy results revealed the influence of MnO on glass matrix. Decrease of B–O bond-related band intensities has been observed. MnO addition was found to introduce broken $[\mathrm{BO_2O^-}]_n$ chains. Differential scanning calorimetry (DSC) measurements presented decreasing T_g that indicates depolymerization of glass matrix in the considered compositional range. Moreover, thermal stability (TS) parameter has been evaluated using the DSC technique. It slightly decreased with MnO content. X-ray photoelectron spectroscopy results provided the evidence for Mn^{2+} and Mn^{3+} presence. Multiplet splitting, close to that of MnO, has been observed. It has been concluded that most of the manganese ions existed in the divalent state. Photoluminescence study revealed that manganese ions are tetragonally co-ordinated in a glassy matrix.

Keywords. Mn; infrared spectroscopy; glass; thermal properties.

1. Introduction

Borate glasses gained significant attention owing to variety of potential applications in modern technology and engineering. For example, they find applications in non-linear optics due to high refractive index induced by high polarizability of dopants such as lead and bismuth [1]. Borate glasses doped with alkali metals are useful in UV range optics owing to their high transparency. Moreover, such glasses possess specific properties for use in sensors and glass fibres [2,3]. Introduction of magnetically active elements gives the possibility of applications in spintronics and magneto-optics [4,5]. Doping with transition metal ions (TMI) seems to be especially interesting. Transition metal oxides such as iron, cobalt and manganese exhibit good solubility in a borate matrix [6–8]. Moreover, TMIs can exist in a number of valance states, which leads to semiconducting properties of obtained materials and related applications in solar energy converters and lasers [9–12].

There are only limited number of publications addressing borate-based glasses consisting of manganese oxide [13,14]. Ardelean *et al* [15] studied B_2O_3–Bi_2O_3–MnO glasses containing up to 50 mol% of MnO. On the basis of EPR data, it was found that Mn^{2+} isolated ions exist in a glass matrix in octahedral symmetry [15]. Another study by Winterstein–Beckmann *et al* [16] focused on MnO–SrO–B_2O_3 glass structure–property correlations. Continuous addition of MnO led to depolymerization of borate matrix and clustering of MnO_6 species. Binary manganese–borate glasses were studied by Kajinami *et al* [17] with the employment of high energy X-ray diffraction and X-ray absorption fine structure techniques. This work suggests a gradual change of BO_3 units to BO_4 units as a result of MnO addition. Manganese ions were found to exist in tetrahedral co-ordination. Kupracz *et al* [18] performed a structural study on MnO–SiO_2–B_2O_3 glass systems and concluded that manganese ions exist mostly in Mn^{2+} state.

However, none of these works consisted of series of binary MnO–B_2O_3 glasses with MnO content over 45 mol%. Possible applications in optical materials, integrated optical devices, magneto-optics and luminescent materials (luminescence of Mn^{2+} ions) require synthesis of glasses with good structural and thermal properties and characterization of such systems. In addition, knowledge about oxidation state of Mn ions is crucial. Co-existing of Mn^{2+} and Mn^{3+} in borate glass can lead to polaron conduction mechanism and semiconducting properties.

In this work, we present a study on novel binary MnO–B_2O_3 glass systems focused on the characterization of structural and thermal properties. MnO influence on the borate glass is discussed and the valance state of manganese ions is examined as well. Considering the aforementioned applications, structural homogeneity, low processing temperatures and good thermal stability (TS) of materials are crucial. Successful synthesis of samples with such properties is presented.

2. Materials and methods

Glass samples of xMnO−(100−x)B_2O_3 (where x = 40, 50 and 60 mol%) composition have been obtained. Appropriate amounts of H_3BO_3 (99.99% from POCH) and MnO (99.99% from POCH) were weighed and mixed in an agate mortar to achieve satisfactory grain size. Obtained mixtures were pre-heated to approximately 300°C for 1 h on a hotplate to remove gases that could eventually hinder the melting process. After removal of the gases, samples were inserted into the furnace and heated gradually to 1000°C in porcelain crucibles. Melts were kept at the same temperature for 30 min. Melting process took place in atmospheric conditions. Subsequently, glasses were quenched on a pre-heated metal plate. Amorphous material was obtained in case of all samples.

X-ray diffraction (XRD) measurements were performed on Philips X'PERT PRO X-ray diffractometer with Cu-Kα radiation (λ = 0.154 nm) in the range of 2θ = 10−80°C.

Differential scanning calorimetry (DSC) measurements were performed on NETZSCH STA 449F1. During every measurement, grounded 5 mg samples were placed in cleaned platinum–rhodium crucibles. Heating rate of each sample equalled 15°C min^{-1}. Measurements were performed in argon atmosphere.

Fourier transform infrared spectroscopy (FTIR) results were obtained with Perkin-Elmer Frontier MIR/FIR spectrometer with TGS detector. Each sample was crushed in agate mortar until a fine grain size was achieved. Afterwards, crushed samples were mixed with potassium bromide to acquire 1:100 (sample:KBr) ratio for each sample in order to perform the measurements trough pellet method. Samples were dried in an electrical drier for few hours in order to remove the residual water content. Mixtures of glass and KBr were pressed on hand press to obtain transparent pellets. The spectra were taken in the range of 550–4000 cm^{-1} with a 2 cm^{-1} resolution.

X-ray photoelectron spectroscopy analysis (XPS) was carried out with X-ray photoelectron spectrometer (Omicron NanoTechnology) with 128-channel collector. Investigated samples were pre-cleaned by Ar ion beam. XPS measurement was performed at room temperature in ultra-high vacuum conditions, below 1.1 × 10^{-8} mbar. The photoelectrons were excited by an Mg–Kα X-ray source. The X-ray anode was operated at 15 keV and 300 W. Omicron Argus hemispherical electron analyser with a 4 mm round aperture was used for analysing of emitted photoelectrons. The binding energies were corrected using the background C1s line (285.0 eV) as a reference. XPS spectra were analysed with Casa-XPS software using a Shirley background subtraction and Gaussian–Lorentzian curve as a fitting algorithm.

Photoluminescence spectra (PL) were collected in the 515–750 nm range in case of emission spectra and 320–500 nm for excitation spectra with the employment of Perkin Elmer LS 55 spectrofluorometer. Measurements were performed using pellet samples mixed with KBr in weight ratio of 1:1.

3. Results

3.1 *XRD measurements*

X-ray diffraction results are shown in figure 1. Obtained XRD spectra possess two wide humps in 2θ = 20−40°C and 40–60°C regions, indicating the absence of long range periodicity in considered samples. No sharp Bragg peak is detected in any pattern confirming lack of any crystallinity due to sufficient cooling rate during the quenching process.

3.2 *DSC results*

Differential scanning calorimetry spectra of binary manganese–borate glass samples are presented in figure 2. Glass transition temperature shifts to lower values with increasing MnO amount. Results presented in table 1 show decrease of T_g with increasing amount of dopant. Spectrum of 50MnO–50B_2O_3 sample possess one crystallization peak at approximately

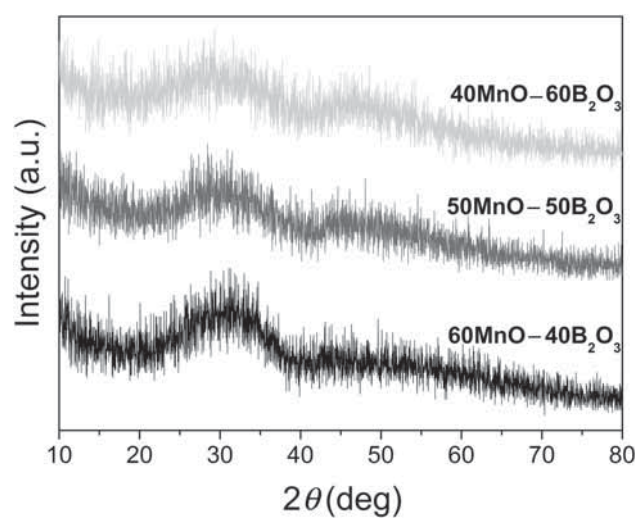

Figure 1. XRD spectra of obtained manganese–borate glass samples.

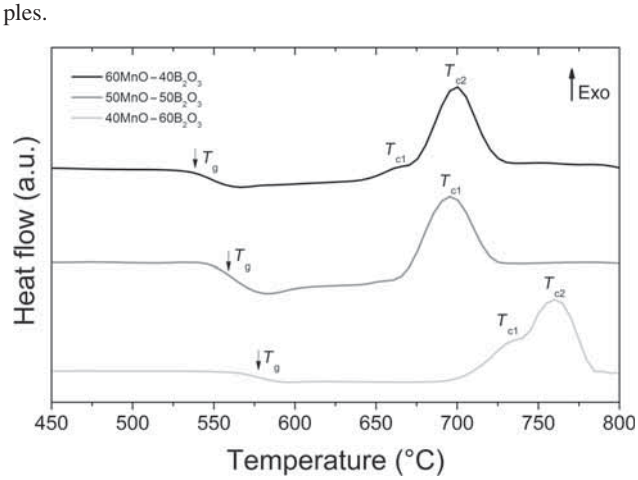

Figure 2. DSC spectra of xMnO−(100−x)B_2O_3 glass samples.

MOST WIEDZY Downloaded from mostwiedzy.pl

Table 1. Thermal parameters of manganese–borate glass samples.

Sample	T_g (°C) ± 2°C	T_{conset} (°C) ± 2°C	T_{c1} (°C) ± 2°C	T_{c2} (°C) ± 2°C	TS ± 2°C
$60MnO–40B_2O_3$	540	646	662	699	106
$50MnO–50B_2O_3$	558	667	696	—	109
$40MnO–60B_2O_3$	577	701	735	761	124

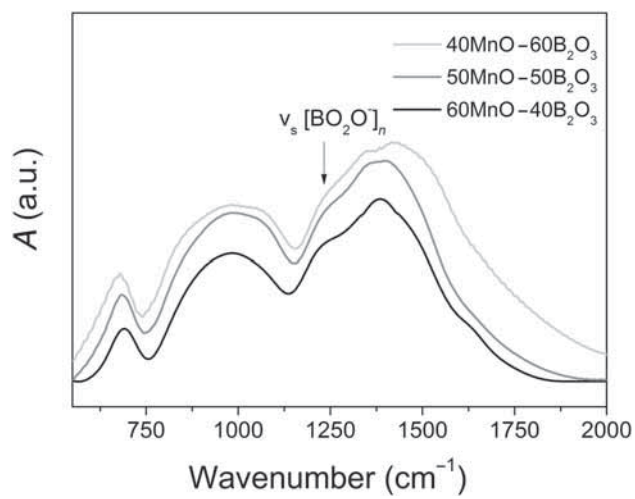

Figure 3. The obtained FTIR spectra of binary manganese–borate glass. Shoulder indicated with an arrow.

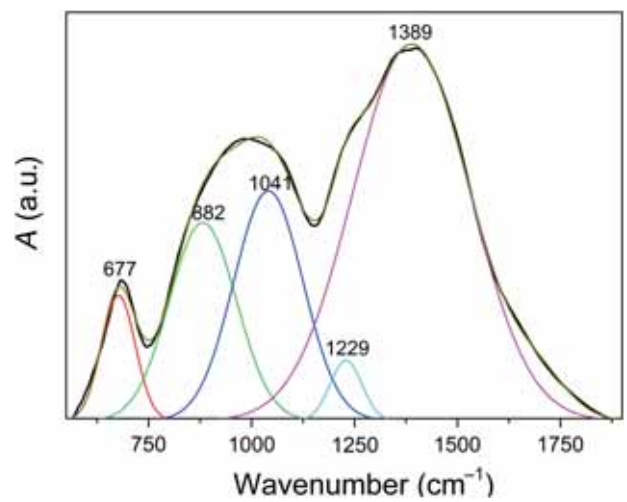

Figure 4. Fitted plot of $50MnO–50B_2O_3$ sample. Gauss functions visualized.

680°C. In case of $40MnO–60B_2O_3$ and $60MnO–40B_2O_3$ samples existence of two exothermic peaks (denoted as T_{c1} and T_{c2}) is confirmed. The presence of both T_{c1} and T_{c2} exothermic signals suggest coexistence of two crystalline phases in a considered temperature regime. In addition, with increasing MnO amount shift of T_{c1} and T_{c2} peaks to lower temperature values is observed.

Based on DSC results, TS is determined. It is expressed by TS parameter according to the equation introduced by Dietzel [19]:

$$TS = T_{conset} - T_g \quad (1)$$

where TS is thermal stability, T_{conset} is the onset of the first crystallization peak and T_g is glass transition temperature. Measurement results show that influence of MnO on TS of prepared samples is evident. TS parameter slightly decreases with increasing MnO.

3.3 *FTIR study*

Due to the complexity of the manganese–borate glass structure, it was necessary to perform FTIR measurements to describe alterations caused by an MnO addition. Figure 3 shows acquired FTIR spectra of manganese borate samples. Each spectrum possesses three main bands [11,12,18]. Beginning with low wavenumber values one can notice a narrow band at approximately 680 cm^{-1} as a result of B–O–B bending vibrations. Wide signal in 750–1100 cm^{-1} range is caused by stretching vibrations of B–O bonds in BO_4 tetrahedrons from various borate groups. Finally, B–O stretching in $[BO_2O^-]_n$ chains is the origin of the last band at 1150–1500 cm^{-1}. Shoulder indicated with an arrow symbol increases with increasing MnO content. This may suggest the increasing number of broken borate chains since the shoulder originates from B–O stretching of $[BO_2O^-]_n$ species.

Fitted spectrum is presented in figure 4. Gaussian curve fitting algorithm has been used. Peak centres obtained in that manner were used in further interpretation. Detailed results are presented in table 2.

3.4 *XPS study*

X-ray photoelectron spectroscopy spectra for Mn2p and Mn3s regions are presented in figures 5 and 7, respectively. Figure 5 shows a doublet in Mn2p region. Two peaks are related to $Mn2p_{3/2}$ (642 eV) and $Mn2p_{1/2}$ (654 eV). The $Mn2p_{3/2}$ peaks are asymmetric due to the presence of a slight and broad shake-up peak close to 647 eV, whereas $Mn2p_{1/2}$ peaks are symmetric and could be fitted by one Gaussian–Lorenzian

MOST WIEDZY Downloaded from mostwiedzy.pl

Table 2. FTIR analysis results and peak positions (C).

Vibration	C (cm^{-1})		
	$40MnO–60B_2O_3$	$50MnO–50B_2O_3$	$60MnO–40B_2O_3$
B–O–B bending [11,12,16]	667	677	689
B–O stretching in BO_4 in diborate groups [11,12,16]	870	882	872
B–O stretching in BO_4 of tri-, tetra- and pentaborate groups [11,12,16]	1037	1041	1009
B–O stretching in $[BO_2O^-]_n$ chains [11,12,16]	1249	1229	1219
B–O^- stretching of $[BO_2O^-]_n$ chains [11,12,16]	1429	1389	1391

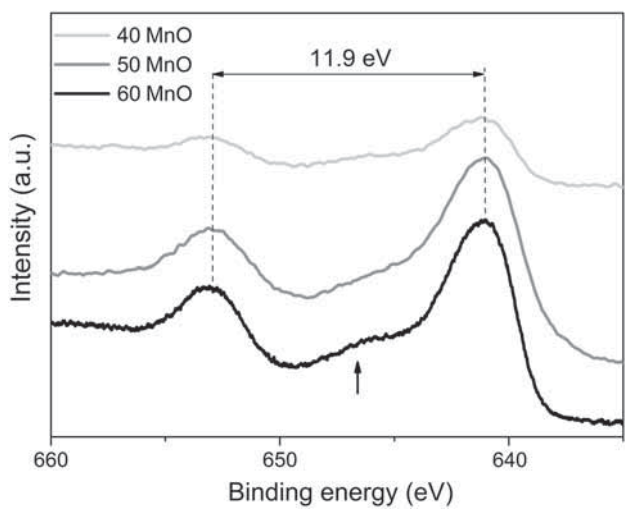

Figure 5. The obtained XPS spectra of Mn2p region. Satellite features are indicated with an arrow.

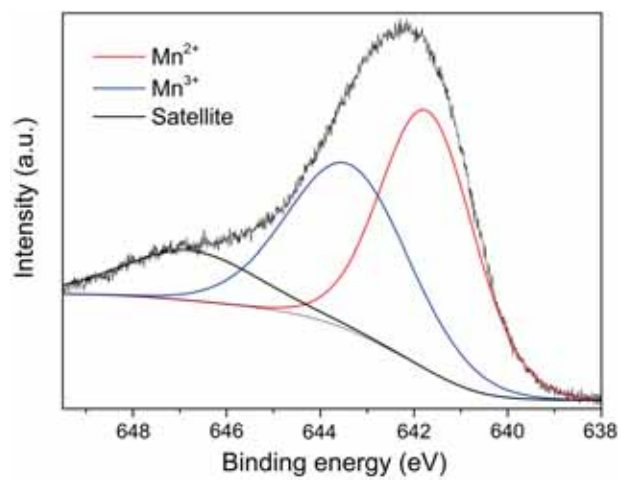

Figure 6. Peak deconvolution for $60MnO–40B_2O_3$ glass sample.

curve. The presence of the shake-up peak, the value of the splitting and the positions of $Mn2p_{3/2}$ and $Mn2p_{1/2}$ peaks suggest that the manganese occurs mainly as Mn^{2+} ions [20,21]. In figure 6, peak de-convolution for $60MnO–40B_2O_3$ glass system is presented. For this sample the highest intensities of Mn2p peaks have been obtained. The peak at 641.5 eV is due to Mn^{2+} presence and the peak observed at 643 eV is assigned to Mn^{3+} ions. Peak due to Mn^{2+} possess higher intensity than signal caused by Mn^{3+} ions. At 647 eV a broad signal is observed, which is probably a satellite feature.

The obtained result is consistent with some other study [15] confirming that in highly doped borate glasses manganese can exist mostly in Mn^{2+} state. In addition, in figure 7 spectra for Mn3s region are presented. Mn3s peaks have two multiplet split components. Splitting between peaks is approximately 6 eV. It clearly indicates the presence of Mn^{2+} ions in investigated glasses [22,23]. However, the presence of some amount of Mn^{3+} can be detected.

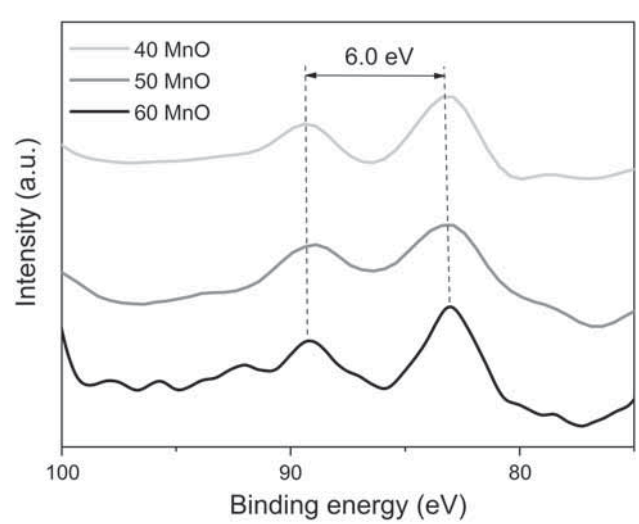

Figure 7. The obtained XPS spectra of Mn3s region.

3.5 *PL measurements*

Borate glasses doped with Mn^{2+} have potential applications as light emitters. Luminescence of these ions varies from green to red colour and is dependent on local symmetry of manganese. Thus, PL studies were performed to determine the performance of obtained samples and to give an insight about Mn^{2+} presence and coordination. Results are presented in figure 8 and excitation spectra of all samples are presented (left). It is worth noting that electronic states

MOST WIEDZY Downloaded from mostwiedzy.pl

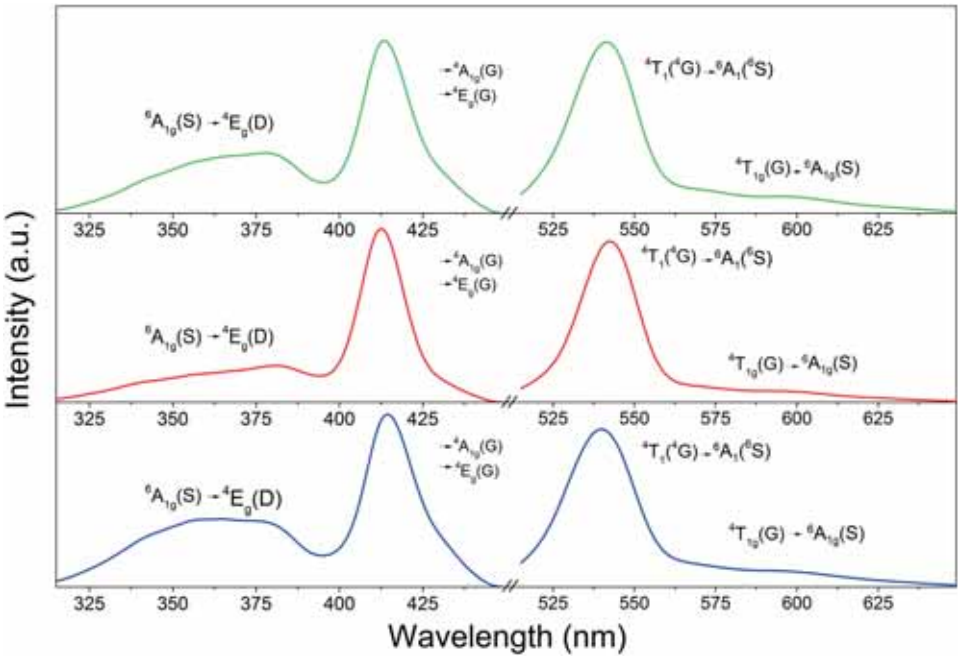

Figure 8. Results of photoluminescence measurements of obtained glass samples with different manganese content (40, 50 and 60 MnO).

of Mn^{2+} ions are affected by a crystal field [24]. Relatively narrow bands are observed in the excitation spectra due to the presence of 4A1g and 4Eg transitions. First, excitation band of low intensity observed at approximately 365 nm has its origin in $^4A_{1g}(S) \rightarrow {}^4E_g(D)$ transition. Second, intensive band positioned at 413 nm is composed of two peaks due to $^4A_{1g}(S) \rightarrow {}^4A_{1g}(G)$ and $^4A_{1g}(S) \rightarrow {}^4E_g(G)$ transitions. Emission spectra of binary $MnO–B_2O_3$ glass samples are presented in figure 8 (right side). Broad, high intensity band that can be observed at approximately 540 nm is a result of $^4T_1(G) \rightarrow {}^6A_1(S)$ radiative transition, which yields green emission. Second, low intensity band at 600 nm can be noticed. Manganese $^4T_{1g}(G) \rightarrow {}^6A_{1g}(S)$ transition is the source of this signal [25].

4. Discussion

X-ray diffraction results presented an amorphous halo. Thus, it is concluded that no long range order exists in studied samples confirming an amorphous character of obtained samples.

Acquired DSC measurement results show that both decreasing of T_g value and shift of the exothermic peaks to lower temperatures indicates degradation of borate glass structure. This process is induced by the addition of transition metal oxide. Decrease of connectivity in a glass matrix leads to observed change of TS as well. However, only slight decrease of TS parameter is observed with increasing manganese content. It might be concluded that after achieving 50 mol% of MnO, borate matrix connectivity was not significantly altered.

From FTIR results it can be deduced that the position of B–O–B bending peak slightly shifts to higher wavenumbers with increasing amount of MnO. Wide band in 750–1100 cm^{-1} is composed of two peaks: one from B–O stretching vibration in BO_4 of diborate groups and the second from B–O stretching vibration in BO_4 of tri-, tetra- and pentaborate groups. These peak centre positions shift with increasing Mn amount. Highest wavenumber value is observed for $50MnO–50B_2O_3$ sample. On the other hand, positions of the two peaks forming the last wide band at 1200–1550 cm^{-1} range are shifting to lower wavenumbers with increasing MnO amount. With addition of MnO, peak intensities are found to decrease as a result of gradual depolymerization of $MnO–B_2O_3$ glass matrix. Moreover, shift of B–O in BO_2O^- group stretching bands to lower wavenumbers is observed. The reason is weakening or elongation of B–O bonds. It is possible that shift of B–O–B bending vibration band is caused by influence of manganese ions. Presence of atoms with larger radius leads to greater energy barrier for bending vibration of B–O–B bonds due to spatial constraints. Shoulder observed at approximately 1230 cm^{-1} (B–O stretching in $[BO_2O^-]_n$ signal) is increasing its intensity with addition of MnO. Introduction of $[BO_2O^-]_n$ species suggest depolymerization of borate chains. This result is consistent with aforementioned DSC measurements that indicated decrease of matrix connectivity.

Presented XPS results confirmed the conclusion that manganese exists in two valance states, i.e., Mn^{2+} and Mn^{3+}. As it can be observed Mn2p peak is composed of two bands caused

MOST WIEDZY Downloaded from mostwiedzy.pl

by the presence of these two valance states. However, Mn^{2+} peak dominates over Mn^{3+} signal. Thus, it is concluded that most of the manganese ions exist in a divalent oxidation state. It is evident that the shake-up feature characteristic for MnO is most intensive for highest MnO content. Splitting among Mn2p photoelectron peaks is approximately 11.9 eV, which is indicative of manganese in a divalent state. In addition, the distance between two Mn3s photoelectron peaks (6.0 eV) corresponds to that characteristic of MnO, confirming that Mn^{2+} state is dominant.

Photoluminescence measurements additionally confirmed the presence of manganese ions in a divalent state. Excitation spectra exhibit characteristic bands of manganese ions. These signals have their origin in $^4A_{1g}(S) \rightarrow {}^4E_g(D)$, $^4A_{1g}(S) \rightarrow {}^4A_{1g}(G)$ and $^4A_{1g}(S) \rightarrow {}^4E_g(G)$ transitions. Emission peak due to $^4T_1(G) \rightarrow {}^6A_1(S)$ radiative transition is present at approximately 540 nm. It changes its position slightly shifting to longer wavelengths. An additional low intensity band at 600 nm is noticeable due to 4T1g(G) → 6A1g(S) transition. It has been reported that green emission of Mn^{2+} is indicative of its tetrahedral co-ordination and reddish–orange emission is assigned to octahedrally co-ordinated ions [25]. Considering this it can be concluded that Mn^{2+} ions exist mostly in tetrahedral co-ordination since their most intensive emission peak is located in the green colour region. On the other hand, low intensity red colour transition characteristic to octahedral orientation is observed. It suggests that some portion of manganese ions are octahedrally co-ordinated. No shifts of emission peaks can be noticed, which lead to the conclusion that co-ordination of manganese ions is not significantly changed with increase of manganese content. Thus, highly doped binary manganese–borate glass synthesized in this work is a good example of a green emitter in a wide compositional range.

5. Conclusions

Binary, amorphous manganese–borate glass samples with high manganese content (40, 50 and 60 mol% of MnO) were successfully synthesized. It was possible to melt stable amorphous material. FTIR, XRD, XPS and DSC techniques were employed to study obtained glass samples. As it was shown, MnO addition to borate glass has significant influence on structure and thermal properties of modified material. It has been concluded that gradual addition of MnO causes alterations of matrix structure, mainly breaking of borate chains to form $[BO_2O^-]_n$ species. Matrix depolymerization is supported by DSC results showing decrease of glass transition temperature with MnO addition. However, introduction of MnO caused only a slight decrease in TS of the obtained glasses. The XPS study revealed that manganese exists mostly in Mn^{2+} form. PL spectra confirmed the presence of Mn^{2+} ions. According to obtained results, most of the ions were tetrahedrally coordinated. The obtained low cost glass with its good structural and thermal properties is interesting material for further studies in terms of electronic and optoelectronic applications employing Mn^{2+} and Mn^{3+} ions.

References

[1] Singh N, Singh K J, Singh K and Singh H 2004 *Nucl. Instrum. Methods Phys. Res. Sect. B Beam Interact. Mater. Atoms* **225** 305

[2] Marzouk S Y, Soliman L I, Gaafar M S, Zayed H A and El-deen A H S 2012 *J. Appl. Sci. Res*. **8** 2325

[3] Zhou Y, Gai N, Wang J, Chen F and Yang G 2009 *J. Lumin.* **129** 277

[4] Pal M 2011 *J. Mod. Phys*. **2** 1062

[5] Kliava J, Edelman I, Ivanova O, Ivantsov R, Petrakovskaja E, Hennet L *et al* 2011 *J. Magn. Magn. Mater.* **323** 451

[6] Wen H and Tanner P A 2015 *J. Alloys Compd*. **625** 328

[7] Moustafa F A, Fayad A M, Ezz-Eldin F M and El-Kashif I 2013 *J. Non-Cryst. Solids* **376** 18

[8] Rajyasree C and Rao D K 2011 *J. Non-Cryst. Solids* **357** 836

[9] Steudel F, Loos S, Ahrens B and Schweizer S 2015 *J. Lumin.* **164** 76

[10] Ekdal E, Garcia Guinea J, Karabulut Y, Canimoglu A, Harmansah C, Jorge A *et al* 2015 *Appl. Radiat. Isot.* **103** 93

[11] Chen D, Xiang W, Liang X, Zhong J, Yu H, Ding M *et al* 2015 *J. Eur. Ceram. Soc.* **35** 859

[12] Vázquez G V, Muñoz H G, Camarillo I, Falcony C, Caldiño U and Lira A 2015 *Opt. Mater. (Amst)* **46** 97

[13] Dzhavadyan V G, Edoyan R S and Gukasyan S B 1974 *Stekloobraznoe Sostoyanie* p 129

[14] Sarukhanishvili A V 1979 **5** 530

[15] Ardelean I, Cora S, Ciceo Lucacel R and Hulpus O 2005 *Solid State Sci*. **7** 1438

[16] Winterstein-Beckmann A, Möncke D, Palles D, Kamitsos E I and Wondraczek L 2013 *J. Non-Cryst. Solids* **376** 165

[17] Kajinami A, Kotake T, Deki S and Kohara S 2003 *Nucl. Instrum. Methods Phys. Res. Sect. B Beam Interact. Mater. Atoms* **199** 34

[18] Kupracz P, Karczewski J, Prześniak-Welenc M, Szreder N A, Winiarski M J, Klimczuk T *et al* 2015 *J. Non-Cryst. Solids* **423–424** 68

[19] Dietzel A 1968 *Glass Tech. Berl*. **22** 41

[20] Crist B V 2000 *Handbook of monochromatic XPS spectra* (Chichester: Wiley)

[21] Ehrt D 2013 *Phys. Chem. Glasses. Eur. J. Glas. Sci. Technol. B* **54** 65

[22] Biesinger M C, Payne B P, Grosvenor A P, Lau L W, Gerson A R and Smart R S 2011 *Appl. Surf. Sci.* **257** 2717

[23] van der Heide P A W 2008 *J. Electron Spectroscop. Relat. Phenom.* **164** 8

[24] Wan M H, Wong P S, Hussin R, Lintang H O and Endud S 2014 *J. Alloys Compd.* **595** 39

[25] Gacem L, Artemenko A, Ouadjaout D, Chaminade J P, Garcia A, Pollet M *et al* 2009 *Solid State Sci.* **11** 1854

MOST WIEDZY Downloaded from mostwiedzy.pl